Exciton recombination dynamics in InAs/InP self-assembled quantum wires

David Fuster
Instituto de Microelectrónica de Madrid (CNM-CSIC), Isaac Newton 8, 28760 Tres Cantos, Madrid, Spain

Juan Martínez-Pastor
Instituto de Ciencia de los Materiales, Universidad de Valencia, P.O. Box 22085, 46071 Valencia, Spain

Luisa González and Yolanda González
Instituto de Microelectrónica de Madrid (CNM-CSIC), Isaac Newton 8, 28760 Tres Cantos, Madrid, Spain
(Received 30 August 2004; revised manuscript received 22 December 2004; published 31 May 2005)

In this work we investigate the exciton recombination dynamics in InAs/InP semiconductor self-assembled quantum wires, by means of continuous wave and time resolved photoluminescence. The continuous wave photoluminescence results seem to indicate that the temperature quenching of the emission band seems to be more probably due to unipolar thermal escape of electrons towards the InP barrier. On the other hand, the analysis of time resolved photoluminescence reveals that the temperature dependence of the radiative and nonradiative recombination times is mainly determined by the dynamics of excitons localized by disorder (high energy tail of the PL band) and strongly localized (low energy tail of the PL band) in local size fluctuations of the quantum wires.

DOI: 10.1103/PhysRevB.71.205329 PACS number(s): 78.67.Lt, 78.55.Cr, 78.47.+p

I. INTRODUCTION

Due to the increasing potential applications of semiconductor quantum nanostructures like quantum dots (QDs) and quantum wires (QWRs) for the development of room temperature operating heterostructure lasers and high-speed optoelectronic devices, the carrier trapping and thermal escape processes are of considerable interest. In particular, self-assembled QWRs of InAs grown on InP (001) are good candidates for their use as the active region in optoelectronic devices working at the wavelengths of 1.30 and 1.55 μm at room temperature,[1–3] very useful for fiber telecommunications.

Strong localization effects on the exciton dynamics in quantum wells (QWs) have been reported in the literature, because of their basic and applied interest. Localization traps for excitons are associated to local potential fluctuations due to well width or alloy composition fluctuations.[4,5] In the limit situation of excitons localized in quantum boxes, a negligible variation with temperature of their radiative exciton lifetime is expected.[6] Less work has been devoted to the exciton dynamics as a function of temperature in QWRs, where excitons can be localized at local potential variations due to wire height (more important) and width fluctuations.[7–9] In a quasi-ideal QWR it is well known the square root dependence of the radiative lifetime with the temperature.[7] However, in less homogeneous QWRs, localization of excitons takes place due to the disorder introduced by the lack of uniformity in height and width, resulting in a more complicated dynamics.[8,9] At low temperatures, where the exciton radiative recombination dominates, the exciton dynamics is closer to that observed either in QWs or QDs, depending on the importance (and size) of those potential fluctuations. At high temperatures, where nonradiative recombination of excitons dominates, the existence of accessible localized and near-free states for excitons would imply a three level system that will affect the thermal escape dynamics of carriers between the low-dimensional structures and the barrier.[10]

In this work, we present a study of the exciton dynamics in samples consisting of InAs/InP QWRs with wavelength emission at 1.3 μm (at 300 K), carried out by means of continuous wave photoluminescence (PL) and time-resolved PL (TRPL) measured as a function of temperature, excitation power, and detection energy. The comparison of the PL integrated intensity and decay time results points out to an exciton recombination dynamics limited by strong exciton localization effects.

II. SAMPLES AND EXPERIMENT

The sample under study consist of 1.6 monolayer (ML) thick InAs deposited on InP(001) with a 100 nm thick InP buffer layer grown by molecular beam epitaxy (MBE). The InAs layer was grown at a substrate temperature T_S $=515$ °C, at a growth rate of 0.1 ML/s in a pulsed dynamic way (pulsed In cell sequence: 1 s ON/2 s OFF). The amount of InAs (1.6 ML) corresponds to the critical thickness for QWRs formation, which is detected when the [1–10] reflection high-energy electron diffraction (RHEED) pattern shows the 2D-3D transition.[1,11] Finally, a 20 nm thick cap layer is grown by MBE at a substrate temperature $T_S=515$ °C. Finally, a 20 nm thick cap layer is grown by MBE at a substrate temperature $T_S=515$ °C. More details about this kind of samples can be found in Refs. 2 and 3.

The continuous wave PL experiments were performed by using the 514.5 nm Ar^+ laser line as an excitation source. The PL signal was dispersed by a 0.22 m focal length monochromator and synchronously detected with a cooled Ge photodiode. For time resolved experiments, sample excitation at 730 nm was done by a green-Nd:YAG (Verdi, Coherent) pumped mode-locked Ti:sapphire laser (Mira 900D, Co-

1098-0121/2005/71(20)/205329(7)/$23.00 ©2005 The American Physical Society

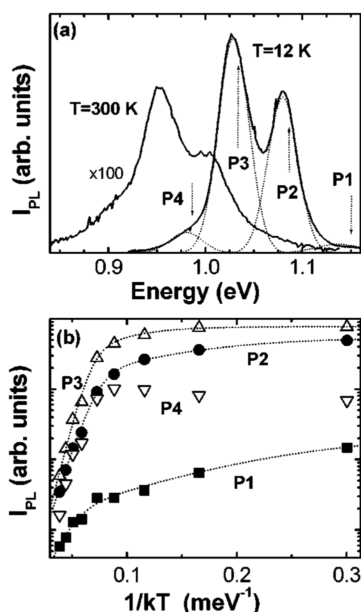

FIG. 1. (a) Continuous lines stand for PL spectra measured at 12 K and at room temperature, and dotted lines correspond to PL-Gaussian components (P1–P4); (b) Arrhenius plot of each PL-Gaussian component integrated intensity (symbols), and the best fitting curves according to Eq. (1) (dotted lines).

herent), providing 2 ps pulses at a repetition rate of 76 MHz. The PL signal was dispersed by a single 0.5 m focal length imaging spectrograph and detected by a synchroscan streak camera (Hamamatsu C5680) with a type S1 cooled photocathode. The overall time response of the system in the widest temporal window (about 2 ns) was around 40 ps (full width at half maximum). In both kinds of experiments the samples were held in the cold finger of a closed-cycle cryostat to vary the temperature in the range 12–300 K.

III. RESULTS AND DISCUSSION

The PL band measured at room temperature is centred at a wavelength of 1.30 μm (0.954 eV), as shown in Fig. 1(a). The PL spectra at the different temperatures can be well reproduced by the sum of four Gaussian bands (dotted lines), as shown in Fig. 1(a) for the PL spectrum at 12 K. These Gaussian components are related to the existence of wire height fluctuations, being the energy difference between two adjacent components consistent with a monolayer fluctuation in the wire height, as established in previous works.[3,12,13] From the viewpoint of the growth procedure, this sample is comparable to the sample grown at 520 °C with an InAs deposited thickness of 0.62 nm, reported by Gendry *et al.*,[14] which doesn't present excited states. Furthermore, the peak energies of the four PL components, labeled P1–P4, as indicated in Fig. 1(a), are consistent with absolute wire heights from 4 to 7 ML, respectively, even if the error in the estimate can be of the order of 2 ML, mainly depending on strain conditions and band offsets.[12] Figure 2 shows the distribution of the wires height obtained from several atomic force microscopy (AFM) images of three uncoated QWRs samples

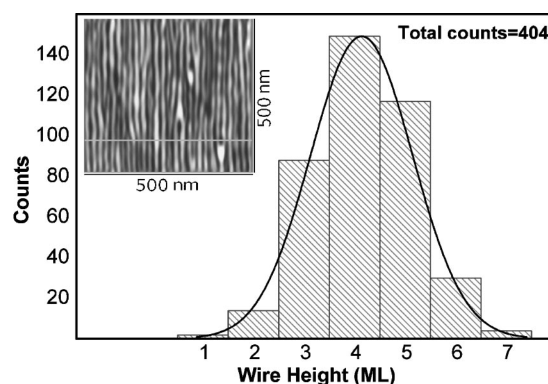

FIG. 2. Gaussian height distribution obtained from atomic force microscopy (AFM) measurements of an uncapped InAs QWRs sample. A 500×500 nm AFM image is shown as an inset.

(grown under similar conditions). The experimental distribution of the wires height is well fitted by a Gaussian centered at a value of 4 ML and having a linewidth around 2 ML. The absolute values of the wire heights measured by AFM could be smaller than the actual ones, given the limitation of the probe tip to penetrate between two wires. Along one QWR we observe height fluctuations of 1–2 ML, coexisting with about 6 ML high quantum dotlike structures (bright areas in AFM images of Fig. 2). Transmission electron microscopy (TEM) observations show that the QWR shape remain after growing the InP cap layer.[2,14] The average dimensions of an InP-capped QWR grown under similar growth conditions as those studied here are 12.9 nm wide and 1.2 nm high.[2] However, TEM data should be also taken as a guide because they are not sensitive enough to discriminate height changes of 1 or 2 ML. The most important fact from the size histogram shown in Fig. 2 is the existence of three main wire families, namely 3, 4, and 5 ML high. These three wire families can be most probably related to the observed PL-Gaussian components P1, P2, and P3 in Fig. 1(a). In this figure, the PL-Gaussian component P3 was the most intense, but it can be due to the larger density of states in P3-family compared to P2 and P1 (more carriers will recombine in bigger wires). The PL-Gaussian component P4 is accounting for the PL lower energy tail, and it is less intense than P2 and P3 components, thus representing the lower concentration of bigger wires and islands (zones of the wires having a larger local height, as some brighter objects observed in the AFM shown as an inset in Fig. 2). Lateral size fluctuations around the average wire width (in the range 9–15 nm) can be responsible of the observed broadening for every PL component, whose typical linewidths are around 25–35 meV.[3,12]

The PL-Gaussian components P1–P4 can be well deconvoluted from the PL band over the entire temperature range. Their respective peak energies exhibit a redshift close to the bandgap shrinkage of bulk InAs. The linewidth of P2–P3 components increases with temperature due to the exciton interaction with acoustic and optical phonons, as occurs in QWs,[15,16] but it takes place at rates below 20 μeV/K in the 12–100 K region. Similar rates are obtained for GaAs/AlGaAs V-groove QWRs.[17] The smaller rates found in QWRs are attributed to the reduction of the confinement

dimensionality (nearly 1D), but in our samples we can also have a certain influence, more difficult to be quantified, of localization centres on the exciton dynamics.

More information about the role of localization centres in the exciton recombination will be obtained by combining the temperature evolution of the PL integrated intensity for P1–P4 and that obtained for the PL decay time. The most probable localization centers for carriers and/or excitons are InAs islands arising from wire height and width fluctuations, although the height is the parameter that determines larger changes in the confinement energy.[12] If the spatial dimensions of these islands are comparable to that of the exciton wave function, the dimensionality of the exciton confinement can be 0D, as occur in the case of well width fluctuations in QWs.[18]

At room temperature, the integrated intensity is two orders of magnitude lower than that measured at 12 K, as was noted in Fig. 1(a). The whole temperature dependence of the PL integrated intensity for the different PL bands is shown in Fig. 1(b). It can be outlined the fact that the integrated intensity of P1–P3 components appreciably decreases in the whole temperature range, whereas that of P4 is practically constant and even increases up to 100 K. The particular behavior of the P4 integrated intensity could be due to either carrier transfer to P4 from the other P1–P3 components via phonon assisted tunneling or recapture of the thermally escaped carriers (from smaller wire families towards the InP barrier). However, we think that it is more realistic associate this effect to the greater error in the determination of the peak energy of this Gaussian on the low energy tail of the PL spectrum (since any resolved band is observed on the low energy tail), which in turn can introduce a subestimation of the PL-quenching energies for the P3-Gaussian component. The observed continuous decrease of the PL intensity can be well reproduced by a two Boltzmann-type quenching mechanisms,[12]

$$I_{\mathrm{PL}}(T) = \frac{I_0}{1 + \tau_0[\Gamma_1 e^{-E_1/kT} + \Gamma_2 e^{-E_2/kT}]}, \qquad (1)$$

where I_0 is the integrated PL intensity at 0 K, E_1 and E_2 are the activation energies of the two quenching mechanisms, Γ_1 and Γ_2 the two related scattering rates, and τ_0 is the radiative recombination time of the excitons in QWR, assumed to be constant and equal to 1 ns for P2, P3 components or 0.5 ns for the P1 component.

These values are taken from our experimental results as we will describe below. Anyway, the consideration of τ_0 as a constant value is not a strong aproximation because at high temperature (above 100 K), where nonradiative recombination is the main contribution, the relevant parameters are E_1 and E_2 in the exponential terms. The best fitting curves (for P1–P3 components) of the experimental results to Eq. (1) are shown in Fig. 1(b) as dotted lines, and the best fitting parameters are listed on Table I. The origin for E_1 activation energies could be some defects (or impurities) in either the wires or their interface with the barrier, as previously suggested.[12] TRPL results will introduce some more light into that preliminary hypothesis. The highest activation energy, E_2, is deduced from the quenching of the PL band at high temperatures (above 100 K), and hence it must be associated to the main nonradiative recombination mechanism in our self-assembled QWRs.[12] It is worth noting that larger values of E_2 are obtained for lower PL energies (see Table I), indicating that carrier escape towards the barrier material (InP in our case) could be the main nonradiative channel. On the one hand, the values found here for E_2 are consistent with the estimate of electron escape energies corresponding to P1–P3 (4–6 ML high wires) PL components by comparing with previous models.[3,12] On the other hand, the activation energies expected for ambipolar carrier escape from the different wire families towards the InP barrier exceed more than 50 meV the values listed on Table I.[19] Nevertheless, the unipolar escape would imply the appearance of an internal electric field preventing this mechanism to be stationary. The potential barrier for electrons would increase to establish a situation that unipolar and ambipolar escape could even compete. That is, that potential barrier and this competition depend on the photogenerated electron-hole concentration. In our experiments, this concentration could be of the order of 10^{10} cm^{-2}, which leads to an internal electric field about 10 kV/cm. Such a value is low enough to consider the electron escape as the main nonradiative mechanism at high temperatures. However, given that we have not the absolute conviction of the actual value of this internal electric field or the possible existence of a 1 ML thick wetting layer, we cannot disregard completely the ambipolar escape mechanism.

TABLE I. Best fitting parameters of the experimental PL integrated intensity (complete band and PL-Gaussian components) as a function of temperature to Eq. (2).

Component/ E_{PL} at 12 K	Γ_1 (s^{-1})	Γ_2 (s^{-1})	E_1(meV)	E_2(meV)
Whole band	2.7×10^9	8×10^{12}	20	140
P3 1.028 eV	8×10^9	2.5×10^{13}	30±10	140±20
P2 1.080 eV	5.5×10^9	9.5×10^{12}	14±4	110±20
P1 1.136 eV	1.7×10^{10}	8×10^{11}	12±2	90±20

It is well known that in many occasions, the activation energies extracted from the temperature dependence of the PL integrated intensity do not reflect the correct exciton dynamics, because it contains both exciton radiative and nonradiative lifetimes.[20] TRPL results are thus necessary in order to have a more complete vision of the exciton dynamics, besides giving us a more accurate measure of the optical quality reached in our samples. Typical PL transients at low temperature registered at the peak energy of the P2 component are shown in Fig. 3(a) for different excitation powers. Below 10 W/cm^2 (around 10 mW of average incident power, approximately) of excitation density, the PL transient is monoexponential, as can be seen in Fig. 3(a). For 100 W/cm^2 the PL transient is also reasonably well reproduced by a monoexponential fit, but with a decay time slightly shorter than that obtained for lower excitation powers. This effect is better observed in Fig. 3(b), where the

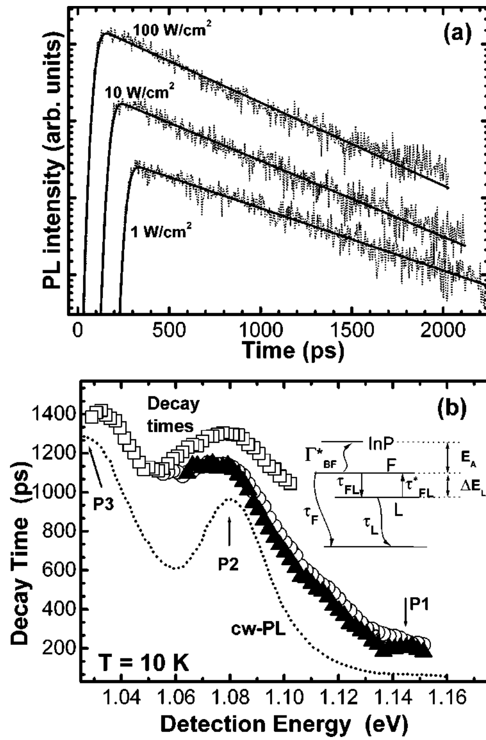

FIG. 3. (a) Dotted lines correspond to experimental PL transients at 10 K for the P2 component measured under different excitation densities. (b) Measured decay time as a function of the detection energy at different excitation densities: 1, 10, and 100 $\mathrm{W/cm^2}$ represented by squares, circles, and triangles respectively. Dotted line reproduces the PL spectrum shown in Fig. 1(a) on the energy range where PL transients have been measured. As an inset, the level scheme applying for the free and localized exciton dynamics with temperature; label "*" in the rate Γ_{BF} and the time τ_{FL} indicates that they are affected with the thermal factor, as written in Eqs. (4) and (5).

effective decay time [that obtained by fitting all PL transients to a single exponential decay, as given in Fig. 3(a)] is plotted against the detection energy of the PL transient. For detection energies above 1.05 eV (P2–P1 emission region) the effective decay time strongly depends on the incident excitation density. The lifetime decreases approximately 200 ps for detecting around P2 peak energy when the excitation density increases from 1 to 10 $\mathrm{W/cm^2}$. This lifetime reduction seems to be more significant for larger detection energies. Nevertheless, above 1.11 eV the PL transients cannot be measured because of the low PL signal. This phenomenology can be a signature of the coexistence of near-free and localized excitons at any emission energy, as was initially observed in QWs.[4,21] In our case, the QWR exhibits height and width fluctuations, the latter contributing to weak disorder effects like in V-grooved wires.[22] On the contrary, height fluctuations can act as more effective exciton localizing centers, because of the stronger local change of the confining potential (around 25 meV per monolayer), in this sense closer to zero-dimensional confinent than one-dimensional with disorder.[23] Following the theory of Citrin,[21] the effective radiative lifetime of excitons (that we can compare with the measured decay time at low temperatures), τ_{rad}, as a function of the localized and near-free exciton population densities, namely L and F, respectively, would be

$$\frac{1}{\tau_{\mathrm{rad}}} = \frac{1}{F+L}\left(\frac{F}{\tau_F} + \frac{L}{\tau_L}\right), \qquad (2)$$

where τ_F and τ_L are the near-free and localized exciton lifetimes, respectively. If we consider τ_F lower than τ_L for every energy at 12 K,[24] we will expect a shorter τ_{rad} by increasing excitation power, because of the finite density of localizing centers. In this sense, τ_{rad} is expected to be less sensitive to excitation power for lower emission energies, because of a larger total areal density of localizing centers (wire height-width fluctuations will lead to lower energy states than those for the average wire dimensions). On the other hand, it is also worth noting the fact that the experimental decay time at a given incident power follows approximately the shape of the continuous wave PL spectrum, as shown in Fig. 3(b). The most reasonable consequence of this fact is that localized exciton recombination is dominating most of the emission band (reflecting the ratio L over $L+F$, mainly), i.e., the mobility edge (energy above which dominates free over localized exciton recombination) would be located on the high energy side of the PL band, somewhere near the P1 peak energy.[4] The measured decay time in the high energy tail quickly decreases as the detection energy increases, up to near one order of magnitude below the values measured at the P2–P3 energy region. This behavior remarks the localization of excitons in the lower energy side and the more QWR-like recombination in the higher energy side,[8] as we will show in detail below from the temperature dependence of the radiative and nonradiative exciton recombination times on the low and high temperature ranges, respectively.

The experiments of TRPL as a function of temperature have been performed in detail up to 100 K for various incident powers $(1,10,100\ \mathrm{W\,cm^{-2}})$, whereas only an excitation density of 10 $\mathrm{W/cm^2}$ has been used to measure the PL signal with a reasonable signal-to-noise ratio over the entire temperature range (12–300 K)). We observe that the PL decay time measured at the P2 peak energy decreases slowly with increasing temperature from 12 to 300 K, as shown in Fig. 4(a). This slow decrease is in contrast to the fast quenching of the continuous wave PL band observed above 100 K [Fig. 1(b)]. We consider interesting to separate the radiative and nonradiative contributions to the PL decay time, because it is clear from Figs. 1(b) and 4(a) that nonradiative recombination is contributing from the lowest temperature. In fact, what one expects is that the radiative recombination time will increase proportional to the square root of the temperature in QWRs. So, the results plotted on Figs. 1(b) and 4(a) tell us that nonradiative recombination channels are opened from the 12 K, in order to compensate that expected increase of τ_{rad}.[24] Let us remember here the above discussion of the results shown in Fig. 1(b), where the small values of the E_1 activation energy make possible an appreciable PL quenching between 12 and 100 K. Separating the radiative and nonradiative contributions, the decay rate is given by

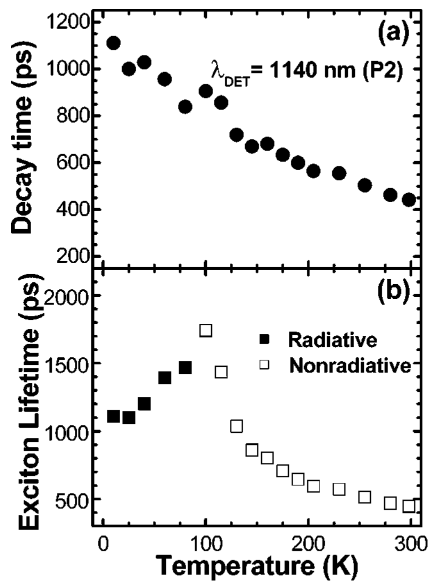

FIG. 4. (a) Temperature evolution of the decay time deduced from the monoexponential PL transients measured for P2 Gaussian component, and (b) estimation of the radiative and nonradiative recombination times as explained in the text.

$$\frac{1}{\tau(T)} = \frac{1}{\tau_{\mathrm{rad}}(T)} + \frac{1}{\tau_{\mathrm{nrad}}(T)} \tag{3}$$

and the temperature dependence of the continuous wave PL intensity can be written as

$$I(T) = I_0 \frac{\tau(T)}{\tau_{\mathrm{rad}}(T)}. \tag{4}$$

If we assume that purely radiative recombination only occurs at the lowest temperature (T=12 K), I_0=I (12 K), we will obtain radiative and nonradiative components at each temperature by using Eqs. (3) and (4) and the experimental values for $I_{\mathrm{PL}}(T)$ and $\tau(T)$ [plotted in Figs. 1(b) and 4(a)], respectively. Figure 4(b) shows the temperature evolution of the radiative and nonradiative recombination times for the emission component P2. Now, we see how the effective radiative exciton lifetime [solid squares in Fig. 4(b)] increases with temperature and determines the decay time up to 100 K. Above 100 K the nonradiative channels are clearly dominant, even though the nonradiative time [hollow squares in Fig. 4(b)] decreases at a slower rate than that expected for electron escape out the QWR towards the InP barrier, which was the mechanism deduced from continuous wave results, as discussed above.

First, let us briefly discuss the temperature dependence of the radiative recombination time below 100 K for 10 and 100 W cm^{-2} (hollow and solid symbols, respectively), as shown in Fig. 5(a) for three different detection energies (approximately those corresponding to P1, P2, and P3 peak energies, $E_{\mathrm{P1}} > E_{\mathrm{P2}} > E_{\mathrm{P3}}$). The temperature evolution of the radiative exciton lifetime is not dependent on excitation power for each PL component. The incident power mainly affects to the absolute values of decay times measured for the P1-Gaussian component, as was discussed above [Fig. 3(b)].

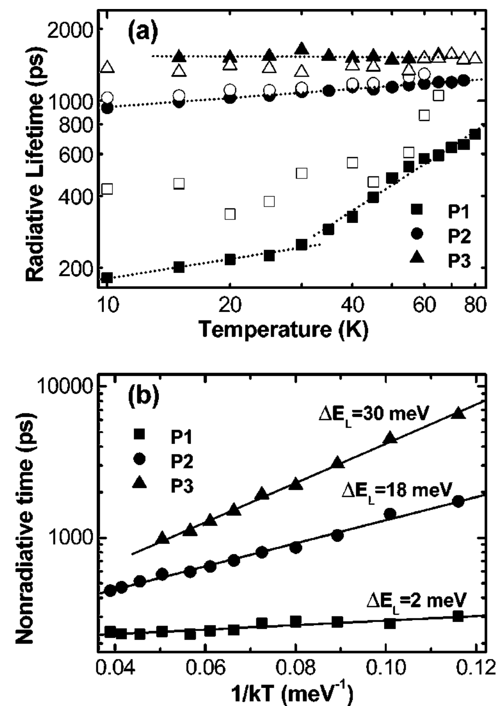

FIG. 5. (a) Logarithmic plot of the radiative recombination time against temperature for P1 (squares), P2 (circles), and P3 (triangles) detecting energies at 10 (hollow symbols) and 100 W/cm^2 (solid symbols); dotted lines stand for the best fit to a T-power law. (b) Arrhenius plot of the nonradiative time for P1–P2–P3 Gaussian components (solid symbols) and the best fit to an energy activated law (continuous lines).

The evolution of the radiative lifetime of the P1 PL peak with temperature in the low temperature range is very similar to that obtained in GaAs V-grooved QWR by Oberli and co-workers.[9] However, this is not the case for the temperature dependence of the exciton radiative recombination time for lower detection energies (P2–P3 region). Dotted lines in Fig. 5(a) represent the best fit of the experimental data to a potential law accounting for the increase of the radiative recombination time. For detection at E_{P3} we can say that the T-exponent is practically zero. For detection at E_{P2} the T-exponent is around 0.125. For detection at E_{P1}, the average T-exponent is 0.5, being 0.27 below 30 K and 0.77 above 30 K, corresponding to the two dotted lines depicted in Fig. 5(a). The average T-exponent for the exciton lifetime measured at E_{P1} is close to what is expected for near-free excitons in QWRs.[7,24,25] However, the observed behavior of a slow increase at low temperatures is expected when disorder effects in QWR are important ("large potential amplitude" and "short potential correlation length"), as calculated for V-grooved wires.[22] On the opposite side, the PL measured at energies below 1.06 eV (P3 component) is completely dominated by recombination of strongly localized excitons, thus having a character closer to what is observed for quantum dots: temperature independent exciton lifetime.

Secondly, in order to better describe the free and localized exciton dynamics, we prefer to use here a simple kinetic model, instead of a more complicated one based on the existence of a mobility edge at certain energy within the PL

band,[4] as we made in previous work for explaining exciton localization in InGaP/GaAs QWs.[5] Our model is based on a three energy level system: one for the InP barrier and the other two for the free and localized exciton states (similar to the model proposed in Ref. 10), which is depicted as an inset in Fig. 3(b). Free excitons (F) are generated at a rate G, which eventually can include the PL rise transient (capture and energy relaxation). The free excitons can either recombine radiatively with a time constant τ_F, be captured into localized states at a rate $1/\tau_{FL}$, or escape towards the barrier at a rate Γ_{BF}, with a thermal activation energy E_A. The localized excitons (L) can either recombine radiatively with a time constant τ_L or thermally transform (with an activation energy ΔE_L) into free excitons through the rate $1/\tau_{LF}$. The rate equation system is then

$$\frac{dF}{dt} = -\frac{F}{\tau_F} - (1 - L/N_L)\frac{F}{\tau_{FL}} - F\Gamma_{FB}\exp(-E_A/kT) + L\frac{\exp(-\Delta E_L/kT)}{\tau_{LF}} + G, \tag{5}$$

$$\frac{dL}{dt} = -\frac{L}{\tau_L} - L\frac{\exp(-\Delta E_L/kT)}{\tau_{LF}} + (1 - L/N_L)\frac{F}{\tau_{FL}}, \tag{6}$$

where N_L is the total density of localized states, and $(1 - L/N_L)$ the factor that takes into account possible saturation effects (more probable at lower temperatures for the excitation density used in the experiment). The PL transient would be determined by

$$I(t) = \frac{F}{\tau_F} + \frac{L}{\tau_L}. \tag{7}$$

The expected PL transient would be reproduced by a second order decay function in the most general case, depending on excitation density conditions over the density of localized centers, N_L, and the other parameters in Eqs. (5) and (6). With the assumption of a large quantity of localization centers as compared to the excitation density, the stationary solution of Eqs. (5) and (6) at high temperatures is

$$I \propto \frac{G}{(\tau_{LF} + \tau_L\exp(-\Delta E_L/kT))\left(\frac{1}{\tau_F} + \frac{1}{\tau_{FL}} + \frac{1}{\tau_{LF}} + \Gamma_{FB}\exp(-E_A/kT)\right)}, \tag{8}$$

where the two activation energies ΔE_L and E_A are implied. The experimental PL intensity evolution with temperature shown in Fig. 1(a) can be well fitted to Eq. (8) with the same activation energies shown in Table I obtained from the best fit to Eq. (1). At the same time, if we numerically solve Eqs. (5) and (6) in the case of a large N_L we obtain a PL transient that can be approximately reproduced by a monoexponential decay with a characteristic decay time,

$$\frac{1}{\tau(T)} = \frac{1}{\tau_L} + \frac{\exp(-\Delta E_L/kT)}{\tau_{LF}}, \tag{9}$$

where it is obvious the contribution of the radiative recombination time for localized excitons, τ_L, and the thermal activated nonradiative term characterized by ΔE_L. The physics expressed by Eqs. (8) and (9) means that the thermal activation (ΔE_L) from localized to near-free excitons is determining the TRPL behavior, whereas the thermally activated (E_A) nonradiative recombination of near-free excitons determines the stationary behavior. Finally, to close the circle between transient and steady state PL results, the Arrhenius plot of the experimental nonradiative time for the three different PL components P1, P2, and P3 above 100 K is shown in Fig. 5(b). The best fitting parameters of the experimental results to the nonradiative term in Eq. (9) are given in Table II. The activation energy for localized-to-free exciton transfer, ΔE_L, increases from 2 to 30 meV from the higher (P1) to the lower energy (P3) Gaussian components. On the one hand, the latter value of 30 meV, found in the case of the P3-band, is consistent with changes of the exciton confinement energy by 1–2 ML wire height fluctuations, as assumed above like the more probable centers for strong exciton localization. On the other hand, these values are comparable to the E_1 values (12, 14, and 30 meV) given above for the fit of the PL integrated intensity of the P1, P2, and P3 PL-Gaussian components to Eq. (2), and now they can be clearly associated to ΔE_L. Evidently, the ΔE_L values listed in Table II are more direct and reliable than the E_1 values listed in Table I, which were obtained from the temperature dependence of the continuous wave PL integrated intensity below 100 K. These results also allow us to extract, from the TRPL measurements, approximate values for τ_{LF} (218, 225, 210 ps for the P1, P2, and P3 components, respectively).

IV. CONCLUSIONS

We have studied the exciton recombination dynamics in InAs/InP(001) self-assembled QWRs by continuous and time-resolved PL. The PL emission study reveals that the quenching mechanism limiting the emission of these samples at room temperature is probably due to thermal escape of electrons towards the InP barrier, because ambipolar thermal escape need of the existence of an InAs wetting layer, which is not revealed by optical and structural experiments. The temperature dependence of the radiative and non-radiative

TABLE II. Best fitting parameters of the experimental nonradiative recombination time as a function of the temperature considering an activated behavior, which is determined by the near-free to localized exciton transfer time and the average localization energy in a given QWR family (represented by the different PL-Gaussian components).

Component/ E_{PL} at 12 K	τ_{FL} (ps)	ΔE_L(meV)
P3 1.028 eV	210	30.0
P2 1.080 eV	225	17.5
P1 1.136 eV	218	2.0

recombination time obtained in TRPL experiments indicates an influence of exciton localization effects in the exciton recombination dynamics. We describe the exciton dynamics using a three level rate equation model. This model allow us to extract quantitative information of the carrier recombination process: the average exciton localization energies and the localized to free exciton transfer rates for the different wire size families (each one characterized by a PL-Gaussian component from the whole PL band). These localization energies are larger (30 meV) on the low energy side of the PL band, indicating a high degree of exciton localization (mostly due to wire height flutuations), with a character quasi-zero-dimensional. On the contrary, a small value is found on the high energy side of the PL band, which is attributed to excitons localized by disorder (mostly due to wire width fluctuations), as occur in typical V-grooved wires. This interpretation is consistent with the observed temperature dependence of the exciton lifetime below 100 K: (i) the exciton lifetime is practically constant for emission energies on the low energy tail of the PL band and (ii) the exciton lifetime for emission energies on the high energy tail of the PL band increase with temperature with a rate very similar to that found in patterned and V-grooved wires affected of a certain degree of weak localization by disorder.

ACKNOWLEDGMENTS

This work was partially supported by Spanish MCyT Nanoself Project No. TIC2002-04096-C03 and by the SANDiE Network of excellence (Contract No. NMP4-CT-2004-500101 group TEP-0120).

[1] L. González, J. M. García, R. García, F. Briones, J. Martínez-Pastor, and C. Ballesteros, Appl. Phys. Lett. **76**, 1104 (2000).
[2] D. Fuster, M. U. González, L. González, Y. González, T. Ben, A. Ponce, S. I. Molina, and J. Martínez-Pastor, Appl. Phys. Lett. **85**, 1424 (2004).
[3] D. Fuster, L. González, Y. González, J. Martínez-Pastor, T. Ben, A. Ponce, and S. I. Molina, Eur. Phys. J. B **40**, 433 (2004).
[4] R. Zimmermann and E. Runge, Phys. Status Solidi A **164**, 511 (1997).
[5] C. Rudamas, J. Martínez-Pastor, L. González, A. Vinattieri, and M. Colocci, Phys. Status Solidi C **0**, 1429 (2003).
[6] R. Heitz, I. Mukhametzhanov, A. Madhukar, A. Hoffmann, and D. Bimberg, J. Electron. Mater. **28**, 520 (1999).
[7] H. Akiyama, S. Koshiba, T. Someya, K. Wada, H. Noge, Y. Nakamura, T. Inoshita, A. Shimizu, and H. Sakaki, Phys. Rev. Lett. **72**, 924 (1994).
[8] J. Bellessa, V. Voliotis, R. Grousson, X. L. Wang, M. Ogura, and H. Matsuhata, Phys. Rev. B **58**, 9933 (1998).
[9] D. Y. Oberli, M.-A. Dupertuis, F. Reinhardt, and E. Kapon, Phys. Rev. B **59**, 2910 (1999).
[10] K. Herz, G. Bacher, A. Forchel, H. Straub, G. Brunthaler, W. Faschinger, G. Bauer, and C. Vieu, Phys. Rev. B **59**, 2888 (1999).
[11] H. R. Gutiérrez, M. A. Cotta, and M. M. G. de Carvalho, Appl. Phys. Lett. **79**, 3854 (2001).
[12] B. Alén, J. Martínez-Pastor, A. García-Cristobal, L. González, and J. M. García, Appl. Phys. Lett. **78**, 4025 (2001).
[13] J. Maes, M. Hayne, Y. Sidor, B. Partoens, F. M. Peeters, Y. González, L. González, D. Fuster, J. M. García, and V. V. Moshchalkov, Phys. Rev. B **70**, 155311 (2004).
[14] M. Gendry, C. Monat, J. Brault, P. Regreny, G. Hollinger, B. Salem, G. Guillot, T. Benyattou, C. Bru-chevallier, G. Bremond, and O. Marty, J. Appl. Phys. **95**, 4761 (2004).
[15] Y. J. Chen, E. S. Koteles, J. Lee, J. Y. Chi, and B. S. Elman, SPIE Quantum Well and Superlattice Physics **792**, 162 (1987).
[16] H. Qiang, F. H. Pollak, C. Mo. Sotomayor Torres, W. Leitch, A. H. Kean, M. A. Stroscio, G. J. Iafrate, and K. W. Kim, Appl. Phys. Lett. **61**, 1411 (1992).
[17] H. Weman, M.-A. Dupertuis, E. Martinet, A. Rudra, and E. Kapon, Appl. Phys. Lett. **79**, 4 (2001).
[18] U. Jahn, M. Ramsteiner, R. Hey, H. T. Grahn, E. Runge, and R. Zimmermann, Phys. Rev. B **56**, R4387 (1997).
[19] P. Michler, A. Hangleiter, M. Moser, M. Geiger, and F. Scholz, Phys. Rev. B **46**, 7280 (1992).
[20] M. Gurioli, J. Martinez-Pastor, M. Colocci, C. Deparis, B. Chastaingt, and J. Massies, Phys. Rev. B **46**, 6922 (1992).
[21] D. S. Citrin, Phys. Rev. B **47**, 3832 (1993).
[22] A. Feltrin, J. L. Staehli, B. Deveaud, and V. Savona, Phys. Rev. B **69**, 233309 (2004).
[23] G. Bacher, J. Kovac, K. Streubel, H. Schweizer, and F. Scholz, Phys. Rev. B **45**, 9136 (1992).
[24] D. S. Citrin, Phys. Rev. Lett. **69**, 3393 (1992).
[25] D. Gershoni, M. Katz, W. Wegscheider, L. N. Pfeiffer, R. A. Logan, and K. West, Phys. Rev. B **50**, 8930 (1994).